MULTIDIMENSIONAL ASSOCIATIONS BETWEEN COGNITION AND CONNECTOME ORGANIZATION IN TEMPORAL LOBE EPILEPSY

A PREPRINT

Raúl Rodríguez-Cruces MD
Universidad Nacional Autónoma de México
Instituto de Neurobiología
Querétaro, Querétaro, México
raulrcruces@inb.unam.mx

Boris C. Bernhardt PhD
MICA laboratory
Montreal Neurological Institute and Hospital
McGill University, Montreal Canada
boris.bernhardt@mcgill.ca

Luis Concha MD PhD *
Universidad Nacional Autónoma de México
Instituto de Neurobiología
Laboratory C-13
Boulervard Juriquilla 3001
Juriquilla, Querétaro, México. C.P. 76230
Phone: +521 442 2381054
Querétaro, Querétaro, México
lconcha@unam.mx

JUNE 19, 2019

ABSTRACT

OBJECTIVE. Temporal lobe epilepsy (TLE) is known to affect large-scale structural networks and cognitive function in multiple domains. The study of complex relations between structural network organization and cognition requires comprehensive analytical methods and a shift towards multivariate techniques. The current work sought to identify multidimensional associations between cognitive profiles and structural network signatures in TLE.
METHODS. We studied 34 drug-resistant TLE patients and 25 age- and sex-matched healthy controls. All participants underwent a comprehensive neurocognitive battery and multimodal magnetic resonance imaging, allowing for large-scale connectomics as well as morphological evaluation of hippocampal and neocortical regions. Using canonical correlation analysis, we identified multivariate associations between cognitive profiles and structural network signatures. Our approach was complemented by bootstrap-based clustering to derive cognitive subtypes and associated patterns of macroscale connectome anomalies.
RESULTS. Both multivariate techniques provided converging evidence for a close coupling between cognitive impairments across multiple domains and large-scale structural network compromise in TLE. Cognitive classes presented with an increasing gradient of abnormalities characterized by increasing cortical and subcortical atrophy and less efficient white matter connectome organization in patients with increasing cognitive dysfunction. Notably, cognitive performance was better indexed by network topological features than by morphometric measures.
CONCLUSIONS. Our findings emphasize a close interplay between multidomain cognitive impairment and large-scale network anomalies in TLE, contributing to the understanding of biological factors contributing heterogeneous functional deficits in the condition.

***K*eywords** Epilepsy · Connectome · Cognition · Multivariate · Network Neuroscience

* **Corresponding author**

1 INTRODUCTION

Temporal lobe epilepsy (TLE) is the most common drug-resistant epilepsy in adults and traditionally associated to mesiotemporal sclerosis, a lesion affecting the hippocampus and adjacent mesial structures [1]. In addition to seizures, patients suffer from cognitive impairments that severely impact everyday functioning and wellbeing [2]. In fact, TLE has traditionally been investigated by cognitive neuroscience as an important model to understand human memory and language dysfunction resulting from hippocampal damage [3].

Recent years, fostered by an increasing administration of comprehensive neurocognitive phenotyping batteries and the advent of high-resolution and multimodal neuroimaging, have seen an evolution in our understanding of the cognitive landscape and structural compromise in TLE [4, 5]. At the level of cognitive function, TLE is now recognized to perturb multiple domains not limited to memory and language processing [5, 6]. These findings are paralleled by mounting neuroimaging evidence suggesting diffuse grey and white matter abnormalities beyond the mesial temporal lobe, affecting a distributed network of cortical and subcortical structures as well as their connections [7, 8, 9].

While some studies have shown compromise of both white and grey matter regions in TLE patients relative to the degree of cognitive dysfunction [10, 11, 12, 13, 14], we lack a comprehensive understanding on the association between the extent of network reorganization and overall cognitive performance. Associations between brain structure and cognitive performance are likely complex, particularly when multiple metrics are used for neuroanatomical profiling on the one hand, and cognitive phenotyping on the other hand. Inter-variable collinearities may furthermore challenge interpretability, and variables could lose their weight when tested individually. Multivariate analyses solve this problem by relating all measures in unified and compact models [15, 16]. Although converging evidence suggest an association between network organization and cognitive impairments in TLE [17], virtually no previous research leveraged multivariate techniques to identify salient brain cognition associations in the condition.

We examined the interplay between multidimensional cognitive performance and structural network compromise in TLE patients and healthy controls. All participants underwent state-of-the-art multimodal magnetic resonance imaging (MRI) and neurocognitive assays. Multivariate Canonical Correlation Analysis (CCA) evaluated associations between multi-domain cognitive impairment and structural connectome reorganization. These models were complemented by unsupervised clustering techniques to identify cognitive subtypes in the TLE cohort, for which we identified morphological and network-based signatures. To strengthen robustness and replicability of discovered network substrates of cognitive impairment, we leveraged bootstrap-based stability assessments as well as cross-validation techniques and made all code and data related to our study openly available.

2 MATERIALS AND METHODS

2.1 Participants

We recruited 34 adult ambulatory patients with drug-resistant TLE (Age= 29.7 ± 11.1 years; 22 females) and 24 age- and sex-matched healthy controls (Age= 32.8 ± 12.7 years; 18 females). Our cohort included 12 right TLE, 18 left TLE, and 4 bilateral TLE patients lateralized by seizure history and semiology, inter-ictal EEG recordings, and neuroimaging. All participants were right-handed native Spanish speakers. They did not have MRI contraindications

nor other neurological comorbidities. Clinical features were obtained through a questionnaire-oriented interview upon referral (age at disease onset= 14.4 ± 9.3 years; seizure frequency per month= 4.2 ± 7.1, number of anti-epileptic drugs= 1.6 ± 0.6, 35.2% had a history of febrile seizures). The Ethics Committee of the Neurobiology Institute of the Universidad Nacional Autónoma de México approved this project (protocol code 019.H-RM) and written informed consent was obtained from all participants in the study according to the Declarations of Helsinki.

2.2 Data acquisition

2.2.1 *Cognition*

Details of the cognitive evaluation are described elsewhere [18]. In brief, all participants underwent a comprehensive battery of cognitive tests: Wechsler Adult Intelligence Scale (WAIS-IV) and Wechsler Memory Scale (WMS-IV). We utilized the following index scores: auditory memory (AMI), visual memory (VMI), visual working memory (VWM), immediate memory (IMI), delayed memory (DMI), verbal comprehension (VCI), working memory (WMI), processing speed (PSI), and perceptual reasoning (PRI). All reported indices were normalized relative to a Mexican population and adjusted by age and education level.

2.2.2 *Magnetic Resonance Imaging*

Images were acquired with a 3 Tesla Philips Achieva TX scanner with a 32-channel head coil. T1-weighted volumes (3D-SPGR, three-dimensional spoiled gradient echo) had a voxel resolution of 1x1x1 mm^3, repetition time (TR) of 8.1 ms, echo time (TE) of 3.7 ms, flip angle of 8º, and field of view (FOV) dimensions of 179x256x256 mm^3. Diffusion weighted images (DWI) were acquired with echo-planar imaging (EPI) and a 2x2x2 mm^3 voxel resolution, TR=11.86 s and TE=64.3 ms, and FOV=256x256x100 mm^3. DWI were sensitized to 60 different diffusion gradient directions (b=2000 s/mm^2); one b=0 s/mm^2 volume was also acquired. An additional b=0 s/mm^2 volume was obtained with reversed phase encoding polarity to account for geometric distortion corrections.

2.3 Image processing

2.3.1 Diffusion MRI processing

a) Diffusion weighted volumes (DWI) were denoised based on data redundancy criteria from a principal component analysis approach [19], followed by non-uniform intensity normalization. Reverse phase encoding from two b=0 s/mm^2 volumes was used to estimate and correct for geometric distortions. DWI volumes were linearly registered to the b=0 s/mm^2 images for motion correction and diffusion gradient vectors were rotated according to the transformation matrix [20].

b) Structural connectome parameterization. Using FreeSurfer v5.3.0, MRtrix 3.0, and FSL 5.0.6, we calculated individual structural connectivity matrices based on the corrected DWI and using Spherical-deconvolution Informed Filtering of Tractograms (SIFT [21]) with anatomically constrained tractography models (ACT [22]) A total of 162 nodes were defined merging the cortical parcellation from the Destrieux Atlas [23] and volBrain's subcortical segmentation (*See OSF repository*). Whole brain tractography was first calculated using ACT with 20 million streamlines seeded on the gray-white matter interface, with maximum deviation angle of 22.5º, maximum length of 250 mm, minimum

length of 10 mm. These tractograms were filtered via SIFT to 2 million streamlines. Connection weights between nodes (N_{SIFT}) were defined as the streamline counts following SIFT [24, 25]. This procedure has shown high reproducibility in structural connectomics [26].

Connectivity matrices were analyzed using the *igraph R package* (`igraph.org/r`). We focused on path length, clustering coefficient, and degree centrality, the most widely used graph-theoretical parameters in the TLE literature [27], also given that these measurements offer a compact description of global network topology and local connectivity embedding [28]. We computed *clustering-coefficient (C)* as a measure of segregation, which provides information about the level of local connections in a network. Additionally, we measured the characteristic *path length (L)* as a measure of network integration - with short path lengths indicating globally efficient networks. Dijkstra algorithm was used to calculate the inverse distance matrix and infinite path lengths were replaced with the maximum finite length [29]. Finally, we calculated *degree centrality (k)* to characterize the relevance of the individual nodes.

To assess the stability of network parameters, a proportional threshold was calculated for each subject connectivity matrix by preserving the proportion of the strongest weights. All the other weights and the main diagonal were set to 0. Network parameters (*k, C, L*) were recursively thresholded from 0.1-0.9 to find the appropriate threshold for network metrics reaching convergence stability.

2.3.2 *Structural MRI processing*

a) Hippocampal volumetry. T1-weighted volumes were processed using volBrain (`volbrain.upv.es`), which provides automated patch-based hippocampal and subcortical delineation with high accuracy in controls and TLE [30]. Hippocampi were individually inspected by a trained rater (RC), and hippocampal volumes were normalized by intracranial volume.

b) Cortical thickness analysis. Cortical thickness was measured for each participant using FreeSurfer v5.3.0. T1-weigthed images were pre-processed through non-local-means denoising [31] and N4 bias field correction prior to FreeSurfer segmentation. After processing, pial and white matter surfaces were visually inspected by a trained rater (RC) and corrected if necessary. Individual surfaces were registered to a surface template with 20,484 surface points (fsaverage5) and a surface-based Gaussian diffusion filter with a full width at half maximum of 20mm was applied, similar to our previous studies [32].

2.4 Multivariate Analysis

2.4.1 *Regularized canonical correlation analysis*

Canonical correlation analysis (CCA) assessed multivariate associations between cognitive scores and structural connectome measures (**Figure 1.A, Top**). CCA was recently employed in a large cohort of healthy young adults to identify associations between neuroimaging-based connectivity measures on the one hand, and lifestyle, demographic and psychometric metrics on the other hand [33]. Here, we built a first CCA (CCA_1) to evaluate associations between morphological measures (*i.e.*, volumetric and cortical thickness measures) and cognitive scores. A second CCA (CCA_2) assessed associations between connectome-derived parameters (degree, clustering coefficient, and characteristic path length of all brain regions, concatenated into a one row vector per subject, resulting in a matrix X (*subjects* $\times$ *network measurements*). Among the cognitive parameters, we excluded IQ because of its high correlation with all the remaining

scores, resulting in a matrix Y (*subjects* $\times$ *cognitive measures*).

The main objective of CCA is to estimate canonical variates (U and V) that maximize the correlation between X and Y. Resulting canonical variates can be ordered ($U_1...U_n$, and $V_1...V_n$), with the first explaining the largest proportion of covariance. Additionally, canonical loadings were calculated for each variable of the original sets (X and Y); they represent the linear correlation between an original variable and a canonical variate. As the number of subjects was less than the number of variables in both data sets, we included two regularization parameters, estimated via leave-one-out cross-validation with recursive search (**Figure 1.A, Bottom**). These parameters were employed to reduce overfitting due to the large number of variables [34]. To estimate confidence intervals and significance of the canonical correlations and canonical loadings, after calculating the appropriate regularization parameters, the rCCA model was permuted and bootstrapped 10,000 times.

In addition to the main TLE rCCA model, we evaluated the following additional models to test for specificity: one including only controls, one controlling matrix X and Y for morphological measures (*i.e.*, hippocampal volume and mean cortical thickness), and one including clinical features on the X matrix. The latter was performed to reveal possible clinical contributions to cognitive profiles beyond structural parameters. Finally, we estimated a model with the volumes of the cortical and subcortical structures in X and a full model that included network parameters, clinical features, and volumes.

2.4.2 *Stable cluster analysis for cognitive phenotypes*

Clustering techniques have been suggested to capture heterogeneity in different clinical cohorts [35, 36], and applied to cognitive variables in epileptic groups [4, 5]. We performed a classification based in the cognitive scores of TLE patients in order to seek potential associations between our multivariate analysis and neurocognitive performance. Robust cognitive phenotypes were identified via unsupervised and bootstrap-supported analysis to identify maximally stable clusters (**Figure 1.B**) [37]. In brief, we took the dataset of cognitive scores and TLE lateralization as a numeric input matrix Y. Bootstrap with replacement was applied to Y and we obtained a new set of samples of Y, with each realization defined as Y_{boot}. Next, we applied Ward D2 hierarchical agglomerative clustering to each Y_{boot}, and the optimal number of clusters (k) was determined from $k = 1...30$ [38]. The next step consisted in the generation of the best partition adjacency matrix Y, where $Y_{ij} = 1$ if participants i and j belong to the same partition and 0 otherwise. After 10,000 bootstraps, the clustering stability was quantified as a matrix S, where each pair of subjects (ij) represents the probability of belonging to the same group. To obtain stable clusters, hierarchical agglomerative clustering (HAC) was applied to S using the k with highest probability from the distribution of all partitions obtained from all bootstraps. Bootstrap based clustering converged on a 3-subtype solution in our TLE cohort.

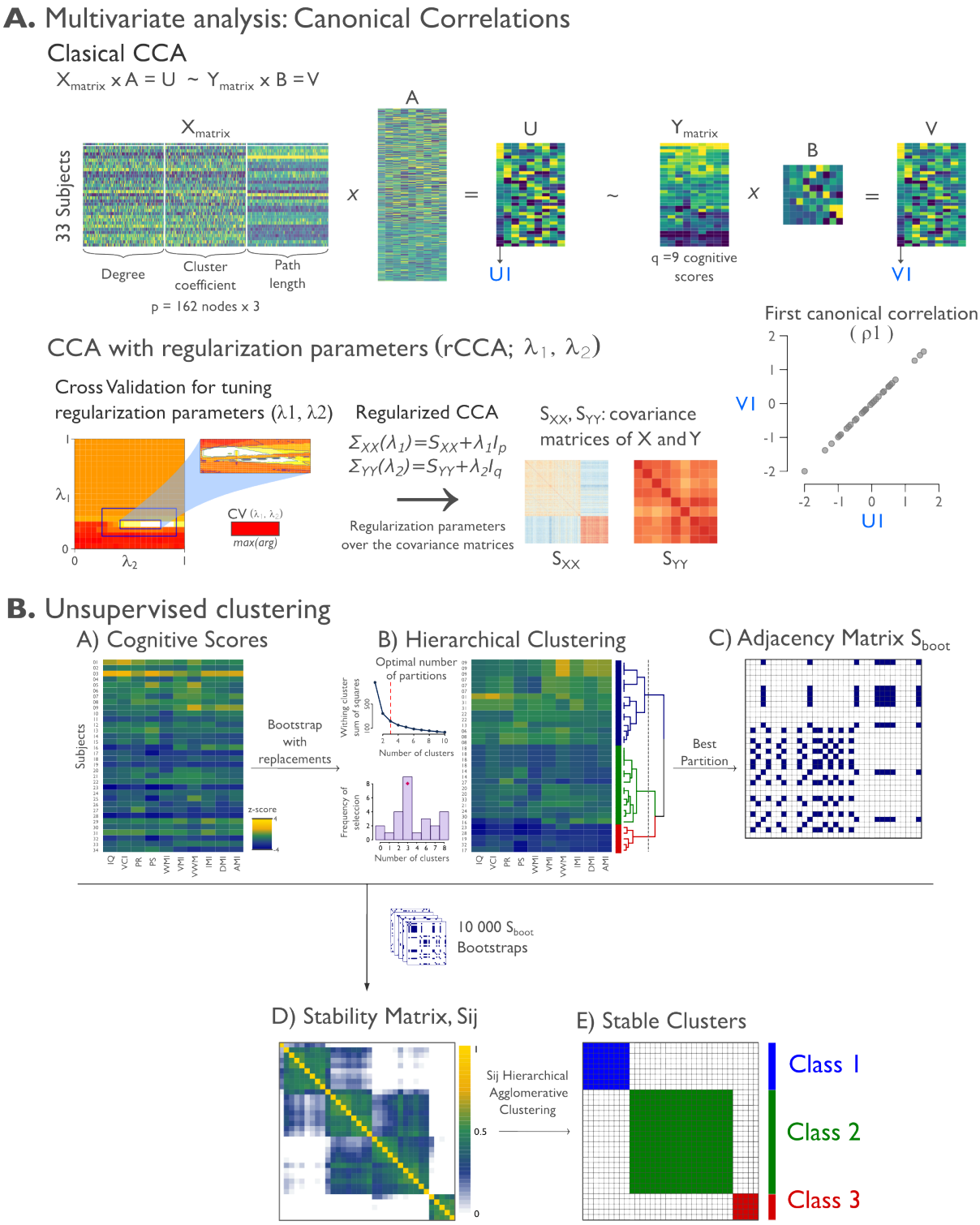

Figure 1: Methods: multivariate analysis and unsupervised clustering. Full text in section 8.1

2.4.3 Class difference analysis

Feature data including hippocampal and subcortical volumes as well as cortical thickness, were z-scored relative to controls and sorted into ipsilateral/contralateral with respect to the seizure focus [39].

a) Clinical variables were compared between classes using ANOVAs followed by Tukey's post-hoc correction for multiple comparisons.

b) Topological complex network. Each nodal parameter (*k, C, L*) was sorted into ipsilateral/contralateral relative to hemispheric TLE lateralization and compared to controls for each Class and represented as effect size (Cohen's D). For statistical comparison, a node-level (ROI) t-test was performed for each TLE class compared to controls. Differences in nodal network parameters were corrected for multiple comparisons at a two-tailed false discovery rate of q=0.05.

*w*ere compared to controls, and corrected with the mean cortical thickness for each subject. Surface-based analysis was done using SurfStat [40]) [available via `http://mica-mni.github.io/surfstat`]. Effect size of the cortical thickness (Cohen's D) between group differences was calculated for each Class, and compared to controls at a vertex level (**Figure 3.C, Bottom**). Vertex-wise statistical comparisons were performed using t-tests, and corrected for multiple comparisons with false discovery rate (FDR) using the Benjamini-Hochberg procedure at q<0.025.

2.5 Data and code availability

Phenotypic and imaging data, as well as code for statistical analysis will be made freely available upon acceptance in our OSF repository: `https:/doi.org/10.17605/OSF.IO/JBDN2`. For processing details, please see: `https://github.com/rcruces/cognition_conectomics_TLE`. For additional information about all rCCA models, the table of ROIs of our segmentations, and further details please see our OSF repository.

3 RESULTS

3.1 Multivariate association analyses

Canonical correlation analysis revealed one significant association between cognitive and structural connectome features in TLE (p<0.05; **Figure 2**). Associated patterns of loadings showed that reduced cognitive scores were related to reduced degree centrality and clustering, together with increased path length. Network loadings encompassed measures from both cortical and subcortical regions and were high in both ipsilateral and contralateral regions. Specifically, longer path lengths were related to lower cognitive scores in TLE, indicating associations between lower global efficiency and worse cognitive performance. Similarly, reduced degree centrality was found in bilateral superior frontal lobes, and precentral gyrus. Finally, clustering coefficient in ipsilateral parietal and middle frontal gyrus related to lower cognitive scores. When clinical and volume features were added to the CCA, results were consistent with the original model, however negative loadings related years of study and volume of both hippocampi with lower cognitive scores.
Multivariate CCA between morphological measures and cognitive characteristics did not yield any significant associations in patients. Likewise, none of the canonical correlations were significant in controls.

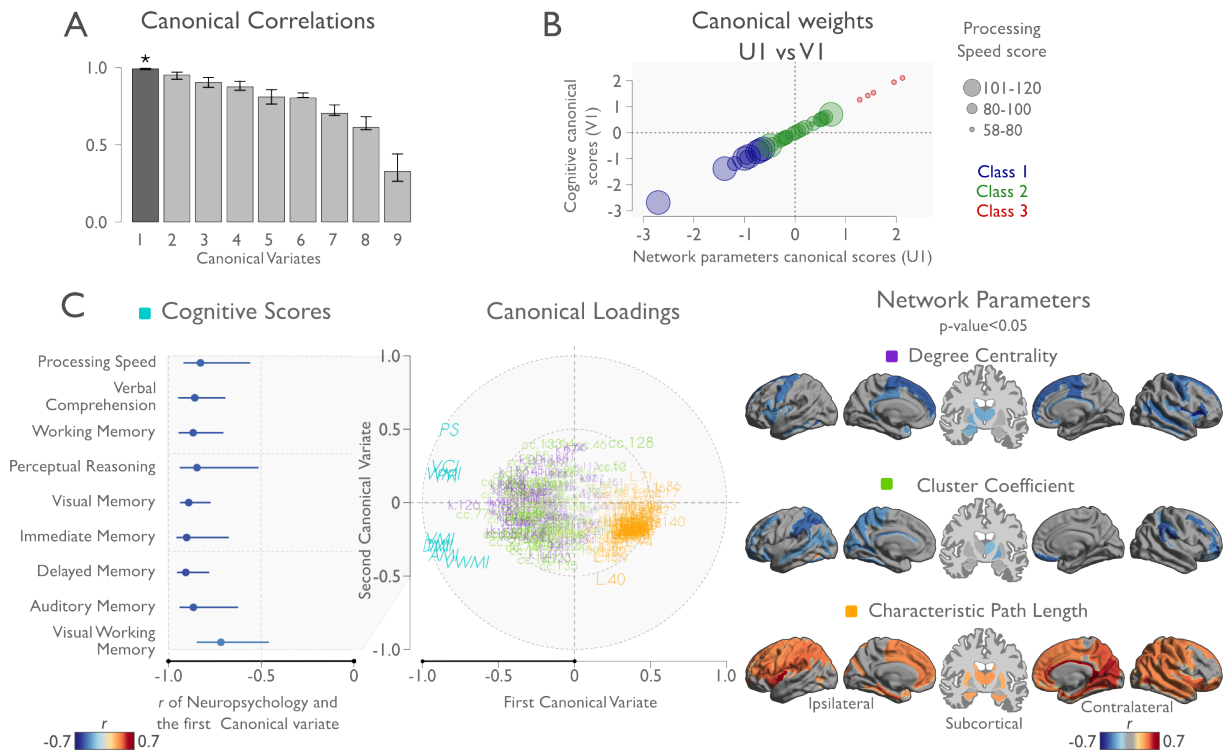

Figure 2: Regularized canonical correlation solution. Full text in section 8.2

3.2 Cognitive Classes

Bootstrap-based clustering of cognitive profiles converged on three cognitive classes in our TLE cohort (**Figure 1.B**, **Figure 3.A**). Cognitive deficits showed an increasing gradient over the three Classes, yet the pattern of these deficits was specific for each. Patients in Class 1 had cognitive scores within normal range, those in Class 2 showed mild impairment in memory-specific domains, and patients in Class 3 displayed pronounced impairment across all domains, with prominent reduction of processing speed.

Class 1 patients presented with older age of epilepsy onset, more years of education, and the shortest disease duration. Despite of these clinical differences, overall findings were similar when controlling for age, duration of epilepsy, and number of antiepileptic drugs. Hippocampal sclerosis was less prevalent in Class 1 (33%) than Class 3 (80%) (**Table 1**).

3.3 Connectome-level and morphological compromise across cognitive Classes

Gradual network organization abnormalities were observed across Classes with most marked changes in Class 3, intermediate differences in Class 2, and only subtle changes in Class 1 (**Figure 3**). Class 1 presented restrained increases of degree centrality and clustering coefficient relative to controls in (ipsilateral) cingulate and parietal cortices at uncorrected thresholds (**Figure 3.B**). Class 2 showed significantly decreased clustering in the contralateral suborbital sulcus and inferior frontal sulcus ($_{pFDR} < 0.025$, **Figure 3.B Middle**). At a connectome-wide level, Class 3 showed the most marked increases of characteristic path length while Classes 1 and 2 were rather normal ($_{pFDR} < 0.025$). In

Class 3, path length increases were most marked in the lateral and medial temporal lobes in both hemispheres, the ipsilateral frontal and the contralateral occipital lobe (**Figure 3.B Bottom**).

Similar to the findings in network parameters, structural MRI markers showed an increasing gradient of changes from Class 1 (the most similar to controls) to Class 3 (the most abnormal, **Figure 3.C**). Hippocampal volumes in Class 1 were within the control range, while Class 2 and 3 had and increasing degrees of hippocampal atrophy (**Figure 3.C Top**). Cortical thinning was also most pronounced in Class 3, particularly in parietal areas ipsilateral to the focus (**Figure 3.C Bottom**).

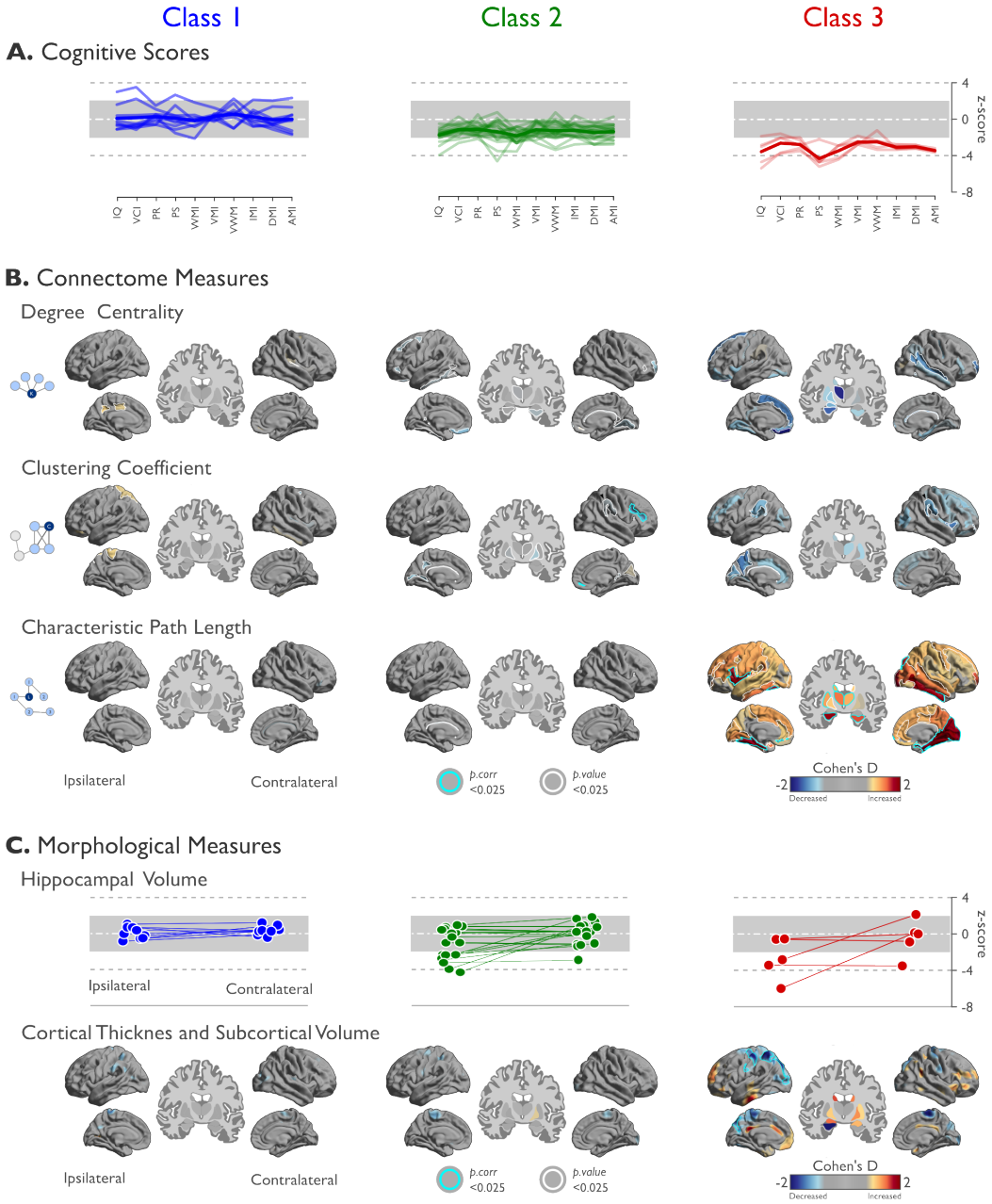

Figure 3: Differences by cognitive class. Full text in section 8.3

4 DISCUSSION

The current work targeted the complex interplay between structural connectome reorganization and cognition in patients with drug-resistant temporal lobe epilepsy (TLE). Harnessing two complementary multivariate data science methodologies – *i.e.*, canonical correlation analysis and data-driven clustering – we observed converging evidence for a close link between the overall degree of white matter network perturbations and multi-domain cognitive impairment in our patients, with overall less efficient network organizations in those with more marked cognitive difficulties. Notably, although complementary cortical thickness analysis also revealed marked morphological anomalies in the same patient cohort, and a subtle correspondence between cognition and the overall degree of grey matter compromise, grey matter measures were less closely associated to cognitive dysfunction than white matter connectome metrics. Furthermore, associations were less marked in healthy controls, suggesting disease specificity. Overall, these findings provide novel and robust evidence for a close and specific coupling of cognitive phenotypes and white matter connectome topology in patients with temporal lobe epilepsy, suggesting a network level pattern underlying broad variations in cognitive function seen in these patients.

Core to our data acquisition was a multidomain cognitive phenotyping together with a whole-brain neuroimaging and connectomics paradigm. The use of a broad neuropsychological battery instead of restricted psychometric testing was motivated by prior observations suggesting that TLE impacts not only language and memory, but rather a diverse set of cognitive domains also including attentional and executive functioning [4, 5]. Similarly, we employed hippocampal volumetry, cortical thickness analyses, as well as diffusion MRI connectomics to assess macroscale brain anomalies in both grey and white matter compartments. Prior histopathological and morphological studies have indeed suggested that although TLE is generally associated to mesiotemporal anomalies [1], it is rarely associated to a confined focal pathological substrate [41, 42]. Instead, an increasing number of MRI-based cortical thickness assessments and subcortical shape analyses have indicated a rather distributed structural compromise, often characterized by bilateral temporo-limbic as well as fronto-central atrophy [7, 9, 32]. Similarly, a growing body of white matter tractographic analyses and network neuroscience work leveraging graph theoretical formalisms of structural connectomes suggested atypical white matter organization and microstructure not limited to the temporal lobe, but in a rather widespread topographic distribution radiating outwards from the mesiotemporal epicenter [10, 14, 43, 44]. Notably, although these distributed abnormalities have been hypothesized to affect cognitive function [2], there are so far only sporadic systematic attempts to relate imaging measures to multidomain cognitive phenotypes in TLE. In fact, among those studies associating structural anomalies and cognitive performance in TLE [11, 12, 13, 14, 18, 45], the majority has been rather selective, focusing on the relation between specific brain measures on the one hand, and specific cognitive domains on the other hand.

To instead integrate the broad panorama of cognitive phenotypes in TLE with a comprehensive array of structural neuroimaging measures, we harnessed multivariate associative techniques as well as bootstrap-based clustering. The former class of models [16], in our case a regularized canonical correlation analysis (rCCA), provides a set of sparse components capturing complex covariation patterns between network parameters and cognitive profiles. A recent study leveraged CCA to identify gradual associations between functional connectome configurations and a wide array of factors related to lifestyle, demographics and psychometric function in a large cohort of young healthy adults, describing a positive-negative mode of co-variation between observable behavior and self-report measures and functional

connectome organization [33]. In our TLE cohort, rCCA revealed a consistent pattern of associations characterized by distributed increases in connectome path length related to reduced cognitive performance. Previous reports have shown similar increases of characteristic path length in this condition compared to controls, suggesting overall reduced global network efficiency [8, 17, 46, 47]. Further elements of the brain-behavior covariation mode encompassed low frontal lobe clustering coefficient together with reduced parietal hubness in patients with reduced cognitive functions, potentially indicating a breakdown of frontal and parietal network segregation that may ultimately reflect network level consequences secondary to microstructural anomalies previously reported in these systems, potentially indicative of axonal damage, myelin alteration, as well as reactive astrogliosis [48, 49]. Notably, as multivariate associative techniques like CCA are prone to overfit, we incorporated several additional elements to ensure specificity and robustness. Firstly, we verified consistency via cross-validation techniques, dispelling potential hyper-optimization of within-sample associations at the expense to out-of-sample generalization. Secondly, we did not observe similar associations in controls, suggesting specificity to TLE. Finally, associations were more marked at the level of white matter connectomes than for grey matter morphometry, confirming overall a close association between white matter connectome architecture and cognitive phenotypes in the condition.

Further support for the consistency of the brain-behavior association in our patients was provided by data-driven clustering of the cognitive profiles, additionally supported in the current work using bootstrap based stability maximization [37]. Subtyping of epileptic patients based on cognitive profiles has previously been employed to demonstrate a spectrum of cognitive function and dysfunction, and to identify subtypes with diverging cognitive strengths and weaknesses [4, 5, 18]. The applied method converged on a three-class solution with gradual cognitive impairments and overall corresponding degrees of brain anomalies, assuring that cognitive impairment in TLE is indeed related to an increased load of white matter connectome reorganization, together with hippocampal and cortical grey matter atrophy. Integrative analyses confirmed that these discovered cognitive classes provide a different viewpoint on the dimensional multivariate mode of covariation seen via CCA. Of note, the prevalence of hippocampal atrophy was found to increase across the three cognitive classes, with the class showing the most marked cognitive dysfunction and connectome anomalies also presenting the highest degree of hippocampal volume loss. Conversely, TLE laterality was similarly distributed across classes, potentially due to the broader range of domains evaluated in the current study than in work focusing on language and/or memory, which generally support more marked impairment in left compared to right TLE [50].

In addition to the novel use of advanced multivariate techniques as well as state-of-the-art connectomics and cognitive phenotyping, our findings are well anchored in overarching assumptions on the link between brain structure and function in healthy and diseased brains. We furthermore made several analytical efforts, including the use of L2 regularization in the CCA, bootstrap-based stability maximization, and cross-validation to minimize overfitting and non-generalizability. Our findings nevertheless lack additional bench testing in independent validation samples that are, however, so far non-existent in the epilepsy imaging literature. Ongoing initiatives such as Enigma-Epilepsy have shown that the pooling of data and analytical resources across different sites is feasible, and that it may lead to consistent findings at the level of grey matter morphology [9]. As a first step towards open epilepsy connectomics, we have made all data and code associated to the current work openly available, promoting independent verification of our findings, further developments, and hopefully a bright future of transparent and reproducible research in the epilepsy neuroimaging field.

5 ACKNOWLEDGEMENTS

We sincerely thank the patients and their families, as well as our control subjects, for their willingness to participate, the medical specialists who helped us with their recruitment, and the clinical personnel at the National Laboratory for magnetic resonance imaging. We are grateful to Juan Ortíz-Retana, Erick Pasaye and Leopoldo González-Santos for technical assistance. We extend our gratitude to the many people who have at some point participated in this study, performing patient recruitment, scanning, and clinical evaluations: Leticia Velázquez-Pérez, David Trejo, Héctor Barragán, Arturo Domínguez, Ildefonso Rodríguez-Leyva, Ana Luisa Velasco, Luis Octavio Jiménez, Daniel Atilano, Elizabeth González Olvera, Rafael Moreno, Vicente Camacho, Ana Elena Rosas, and Alfonso Fajardo. This study was funded by a grant from the Mexican Council of Science and Technology (CONACYT 181508) and from UNAM-DGAPA (IB201712). Raúl Rodríguez-Cruces is a doctoral student from Programa de Doctorado en Ciencias Biomédicas, Universidad Nacional Autónoma de México (UNAM) and received fellowship 329866 from CONACYT. Imaging was performed at the National Laboratory for magnetic resonance imaging, which has received funding from CONACYT (232676, 251216 and 280283). Dr. Bernhardt acknowledges research funding from the National Sciences and Engineering Research Council of Canada (NSERC; Discovery-1304413), Canadian Institutes of Health Research (CIHR; FDN-154298), SickKids Foundation (NI17-039), Azrieli Center for Autism Research (ACAR), an MNI-Cambridge collaboration grant, and salary support from FRQS (Chercheur Boursier).

6 AUTHOR CONTRIBUTIONS

RRC. Conception and design of the study, acquisition and analysis of data, drafting a significant portion of the manuscript and figures.
BCB. Conception and design of the study, drafting a significant portion of the manuscript.
LC. Conception and design of the study.

7 REFERENCES

[1] Ingmar Blümcke et al. "International consensus classification of hippocampal sclerosis in temporal lobe epilepsy: a Task Force report from the ILAE Commission on Diagnostic Methods". In: *Epilepsia* 54.7 (2013), pp. 1315–1329.

[2] Jack J Lin, Marco Mula, and Bruce P Hermann. "Uncovering the neurobehavioural comorbidities of epilepsy over the lifespan." In: *The Lancet* 380.9848 (Sept. 2012), pp. 1180–1192. DOI: 10.1016/S0140-6736(12)61455-X. URL: http://dx.doi.org/10.1016/S0140-6736(12)61455-X (visited on 04/23/2019).

[3] Christian Hoppe, Christian E Elger, and Christoph Helmstaedter. "Long-term memory impairment in patients with focal epilepsy." In: *Epilepsia* 48 Suppl 9 (2007), pp. 26–29. DOI: 10.1111/j.1528-1167.2007.01397.x. URL: http://dx.doi.org/10.1111/j.1528-1167.2007.01397.x (visited on 04/11/2019).

[4] Kevin Dabbs et al. "Neuroanatomical correlates of cognitive phenotypes in temporal lobe epilepsy." In: *Epilepsy & Behavior* 15.4 (Aug. 2009), pp. 445–451. DOI: 10.1016/j.yebeh.2009.05.012. URL: http://dx.doi.org/10.1016/j.yebeh.2009.05.012 (visited on 01/29/2019).

[5] Bruce Hermann et al. "Cognitive phenotypes in temporal lobe epilepsy." In: *Journal of the International Neuropsychological Society* 13.1 (Jan. 2007), pp. 12–20. DOI: 10.1017/{S135561770707004X}. URL: http://dx.doi.org/10.1017/%7BS135561770707004X%7D (visited on 01/29/2019).

[6] C Helmstaedter and C E Elger. "Chronic temporal lobe epilepsy: a neurodevelopmental or progressively dementing disease?" In: *Brain: A Journal of Neurology* 132.Pt 10 (Oct. 2009), pp. 2822–2830. DOI: 10.1093/brain/awp182. URL: http://dx.doi.org/10.1093/brain/awp182 (visited on 04/01/2019).

[7] Jack J Lin et al. "Reduced neocortical thickness and complexity mapped in mesial temporal lobe epilepsy with hippocampal sclerosis." In: *Cerebral Cortex* 17.9 (Sept. 2007), pp. 2007–2018. DOI: 10.1093/cercor/bhl109. URL: http://dx.doi.org/10.1093/cercor/bhl109 (visited on 05/23/2019).

[8] Leonardo Bonilha et al. "Medial temporal lobe epilepsy is associated with neuronal fibre loss and paradoxical increase in structural connectivity of limbic structures". In: *J Neurol Neurosurg Psychiatry* 83.9 (2012), pp. 903–909. (Visited on 05/22/2019).

[9] Christopher D Whelan et al. "Structural brain abnormalities in the common epilepsies assessed in a worldwide ENIGMA study." In: *Brain: A Journal of Neurology* 141.2 (Feb. 2018), pp. 391–408. DOI: 10.1093/brain/awx341. URL: http://dx.doi.org/10.1093/brain/awx341 (visited on 05/22/2019).

[10] Willem M Otte et al. "A meta-analysis of white matter changes in temporal lobe epilepsy as studied with diffusion tensor imaging." In: *Epilepsia* 53.4 (Apr. 2012), pp. 659–667. DOI: 10.1111/j.1528-1167.2012.03426.x. URL: http://dx.doi.org/10.1111/j.1528-1167.2012.03426.x (visited on 01/09/2017).

[11] Beate Diehl et al. "Abnormalities in diffusion tensor imaging of the uncinate fasciculus relate to reduced memory in temporal lobe epilepsy." In: *Epilepsia* 49.8 (Aug. 2008), pp. 1409–1418. DOI: 10.1111/j.1528-1167.2008.01596.x. URL: http://dx.doi.org/10.1111/j.1528-1167.2008.01596.x (visited on 01/29/2019).

[12] C R McDonald et al. "Diffusion tensor imaging correlates of memory and language impairments in temporal lobe epilepsy." In: *Neurology* 71.23 (Dec. 2008), pp. 1869–1876. DOI: 10.1212/01.wnl.0000327824.05348.3b. URL: http://dx.doi.org/10.1212/01.wnl.0000327824.05348.3b (visited on 01/29/2019).

[13] Carrie R McDonald et al. "White matter microstructure complements morphometry for predicting verbal memory in epilepsy." In: *Cortex* 58 (Sept. 2014), pp. 139–150. DOI: 10.1016/j.cortex.2014.05.014. URL: http://dx.doi.org/10.1016/j.cortex.2014.05.014 (visited on 01/29/2019).

[14] Jeffrey D Riley et al. "Altered white matter integrity in temporal lobe epilepsy: association with cognitive and clinical profiles." In: *Epilepsia* 51.4 (Apr. 2010), pp. 536–545. DOI: 10.1111/j.1528-1167.2009.02508.x. URL: http://dx.doi.org/10.1111/j.1528-1167.2009.02508.x (visited on 01/29/2019).

[15] Daniel Zelterman. *Applied Multivariate Statistics with R*. Statistics for biology and health. Cham: Springer International Publishing, 2015. ISBN: 978-3-319-14092-6. DOI: 10.1007/978-3-319-14093-3. URL: http://link.springer.com/10.1007/978-3-319-14093-3 (visited on 04/11/2019).

[16] Anthony R McIntosh and Bratislav Mišić. "Multivariate statistical analyses for neuroimaging data." In: *Annual review of psychology* 64 (2013), pp. 499–525. DOI: 10.1146/annurev-psych-113011-143804. URL: http://dx.doi.org/10.1146/annurev-psych-113011-143804 (visited on 04/11/2019).

[17] Maarten J Vaessen et al. "White matter network abnormalities are associated with cognitive decline in chronic epilepsy." In: *Cerebral Cortex* 22.9 (Sept. 2012), pp. 2139–2147. DOI: 10.1093/cercor/bhr298. URL: http://dx.doi.org/10.1093/cercor/bhr298 (visited on 01/29/2019).

[18] Raúl Rodríguez-Cruces et al. "Association of white matter diffusion characteristics and cognitive deficits in temporal lobe epilepsy." In: *Epilepsy & Behavior* 79 (Jan. 2018), pp. 138–145. DOI: 10.1016/j.yebeh.2017.11.040. URL: http://dx.doi.org/10.1016/j.yebeh.2017.11.040 (visited on 01/29/2019).

[19] Jelle Veraart et al. "Denoising of diffusion MRI using random matrix theory." In: *Neuroimage* 142 (Nov. 2016), pp. 394–406. DOI: 10.1016/j.neuroimage.2016.08.016. URL: http://dx.doi.org/10.1016/j.neuroimage.2016.08.016 (visited on 01/29/2019).

[20] Jesper L R Andersson and Stamatios N Sotiropoulos. "An integrated approach to correction for off-resonance effects and subject movement in diffusion MR imaging." In: *Neuroimage* 125 (Jan. 2016), pp. 1063–1078. DOI: 10.1016/j.neuroimage.2015.10.019. URL: http://dx.doi.org/10.1016/j.neuroimage.2015.10.019 (visited on 01/29/2019).

[21] Robert E Smith et al. "SIFT: Spherical-deconvolution informed filtering of tractograms." In: *Neuroimage* 67 (Feb. 2013), pp. 298–312. DOI: 10.1016/j.neuroimage.2012.11.049. URL: http://dx.doi.org/10.1016/j.neuroimage.2012.11.049 (visited on 01/29/2019).

[22] Robert E Smith et al. "Anatomically-constrained tractography: improved diffusion MRI streamlines tractography through effective use of anatomical information." In: *Neuroimage* 62.3 (Sept. 2012), pp. 1924–1938. DOI: 10.1016/j.neuroimage.2012.06.005. URL: http://dx.doi.org/10.1016/j.neuroimage.2012.06.005 (visited on 01/29/2019).

[23] Christophe Destrieux et al. "Automatic parcellation of human cortical gyri and sulci using standard anatomical nomenclature." In: *Neuroimage* 53.1 (Oct. 2010), pp. 1–15. DOI: 10.1016/j.neuroimage.2010.06.010. URL: http://dx.doi.org/10.1016/j.neuroimage.2010.06.010 (visited on 04/25/2016).

[24] Chun-Hung Yeh et al. "Correction for diffusion MRI fibre tracking biases: The consequences for structural connectomic metrics." In: *Neuroimage* 142 (Nov. 2016), pp. 150–162. DOI: 10.1016/j.neuroimage.2016.05.047. URL: http://dx.doi.org/10.1016/j.neuroimage.2016.05.047 (visited on 01/29/2019).

[25] Robert E Smith et al. "The effects of SIFT on the reproducibility and biological accuracy of the structural connectome." In: *Neuroimage* 104 (Jan. 2015), pp. 253–265. DOI: 10.1016/j.neuroimage.2014.10.004. URL: http://dx.doi.org/10.1016/j.neuroimage.2014.10.004 (visited on 01/29/2019).

[26] Timo Roine et al. "Reproducibility and intercorrelation of graph theoretical measures in structural brain connectivity networks." In: *Medical Image Analysis* 52 (2019), pp. 56–67. ISSN: 13618415. DOI: 10.1016/j.media.2018.10.009. URL: https://linkinghub.elsevier.com/retrieve/pii/S1361841518308569 (visited on 03/25/2019).

[27] Boris C Bernhardt, Leonardo Bonilha, and Donald W Gross. "Network analysis for a network disorder: The emerging role of graph theory in the study of epilepsy." In: *Epilepsy & Behavior* 50 (Sept. 2015), pp. 162–170. DOI: 10.1016/j.yebeh.2015.06.005. URL: http://dx.doi.org/10.1016/j.yebeh.2015.06.005 (visited on 01/29/2019).

[28] Mikail Rubinov and Olaf Sporns. "Complex network measures of brain connectivity: uses and interpretations." In: *Neuroimage* 52.3 (2010), pp. 1059–1069. DOI: 10.1016/j.neuroimage.2009.10.003. URL: http://dx.doi.org/10.1016/j.neuroimage.2009.10.003 (visited on 05/10/2017).

[29] Alex Fornito, Andrew Zalesky, and Edward T Bullmore. "Network scaling effects in graph analytic studies of human resting-state FMRI data." In: *Frontiers in Systems Neuroscience* 4 (June 2010), p. 22. DOI: 10.3389/fnsys.2010.00022. URL: http://dx.doi.org/10.3389/fnsys.2010.00022 (visited on 01/29/2019).

[30] José V Manjón and Pierrick Coupé. "volBrain: An Online MRI Brain Volumetry System." In: *Frontiers in Neuroinformatics* 10 (July 2016), p. 30. DOI: 10.3389/fninf.2016.00030. URL: http://dx.doi.org/10.3389/fninf.2016.00030 (visited on 01/29/2019).

[31] Pierrick Coupé et al. "Patch-based segmentation using expert priors: application to hippocampus and ventricle segmentation." In: *Neuroimage* 54.2 (Jan. 2011), pp. 940–954. DOI: 10.1016/j.neuroimage.2010.09.018. URL: http://dx.doi.org/10.1016/j.neuroimage.2010.09.018 (visited on 05/22/2019).

[32] Boris C Bernhardt et al. "Cortical thickness analysis in temporal lobe epilepsy: reproducibility and relation to outcome." In: *Neurology* 74.22 (June 2010), pp. 1776–1784. DOI: 10.1212/{WNL}.0b013e3181e0f80a. URL: http://dx.doi.org/10.1212/%7BWNL%7D.0b013e3181e0f80a (visited on 02/01/2019).

[33] Stephen M Smith et al. "A positive-negative mode of population covariation links brain connectivity, demographics and behavior." In: *Nature Neuroscience* 18.11 (Nov. 2015), pp. 1565–1567. DOI: 10.1038/nn.4125. URL: http://dx.doi.org/10.1038/nn.4125 (visited on 01/29/2019).

[34] Ignacio González et al. "CCA: An R package to extend canonical correlation analysis". In: *Journal of Statistical Software* 23.12 (2008), pp. 1–14. (Visited on 01/29/2019).

[35] Seok-Jun Hong et al. "Multidimensional neuroanatomical subtyping of autism spectrum disorder." In: *Cerebral Cortex* 28.10 (Oct. 2018), pp. 3578–3588. DOI: 10.1093/cercor/bhx229. URL: http://dx.doi.org/10.1093/cercor/bhx229 (visited on 05/28/2019).

[36] Boris C Bernhardt et al. "Magnetic resonance imaging pattern learning in temporal lobe epilepsy: classification and prognostics." In: *Annals of Neurology* 77.3 (Mar. 2015), pp. 436–446. DOI: 10.1002/ana.24341. URL: http://dx.doi.org/10.1002/ana.24341 (visited on 05/28/2019).

[37] Pierre Bellec et al. "Multi-level bootstrap analysis of stable clusters in resting-state fMRI." In: *Neuroimage* 51.3 (July 2010), pp. 1126–1139. DOI: 10.1016/j.neuroimage.2010.02.082. URL: http://dx.doi.org/10.1016/j.neuroimage.2010.02.082 (visited on 01/29/2019).

[38] Malika Charrad et al. "NbClust Package: finding the relevant number of clusters in a dataset". In: *J. Stat. Softw* (2012). (Visited on 05/22/2019).

[39] Boris C Bernhardt et al. "The spectrum of structural and functional imaging abnormalities in temporal lobe epilepsy." In: *Annals of Neurology* 80.1 (June 2016), pp. 142–153. DOI: 10.1002/ana.24691. URL: http://dx.doi.org/10.1002/ana.24691 (visited on 04/23/2019).

[40] KJ Worsley et al. "SurfStat: A Matlab toolbox for the statistical analysis of univariate and multivariate surface and volumetric data using linear mixed effects models and random field theory". In: *Neuroimage* 47 (July 2009), S102. ISSN: 10538119. DOI: 10.1016/S1053-8119(09)70882-1. URL: https://linkinghub.elsevier.com/retrieve/pii/S1053811909708821 (visited on 04/13/2019).

[41] Francine Blanc et al. "Investigation of widespread neocortical pathology associated with hippocampal sclerosis in epilepsy: a postmortem study." In: *Epilepsia* 52.1 (Jan. 2011), pp. 10–21. DOI: 10.1111/j.1528-1167.2010.02773.x. URL: http://dx.doi.org/10.1111/j.1528-1167.2010.02773.x (visited on 05/29/2019).

[42] Boris C Bernhardt et al. "Imaging structural and functional brain networks in temporal lobe epilepsy." In: *Frontiers in Human Neuroscience* 7 (Oct. 2013), p. 624. DOI: 10.3389/fnhum.2013.00624. URL: http://dx.doi.org/10.3389/fnhum.2013.00624 (visited on 01/29/2019).

[43] Luis Concha, Christian Beaulieu, and Donald W Gross. "Bilateral limbic diffusion abnormalities in unilateral temporal lobe epilepsy." In: *Annals of Neurology* 57.2 (Feb. 2005), pp. 188–196. DOI: 10.1002/ana.20334. URL: http://dx.doi.org/10.1002/ana.20334 (visited on 05/22/2019).

[44] Boris C Bernhardt et al. "Temporal lobe epilepsy: Hippocampal pathology modulates connectome topology and controllability." In: *Neurology* 92.19 (May 2019), e2209–e2220. DOI: 10.1212/{WNL}.0000000000007447. URL: http://dx.doi.org/10.1212/%7BWNL%7D.0000000000007447 (visited on 05/29/2019).

[45] Anny Reyes et al. "Cognitive phenotypes in temporal lobe epilepsy are associated with distinct patterns of white matter network abnormalities." In: *Neurology* 92.17 (Apr. 2019), e1957–e1968. DOI: 10.1212/{WNL}.0000000000007370. URL: http://dx.doi.org/10.1212/%7BWNL%7D.0000000000007370 (visited on 04/09/2019).

[46] A Raj et al. "Network-level analysis of cortical thickness of the epileptic brain." In: *Neuroimage* 52.4 (Oct. 2010), pp. 1302–1313. DOI: 10.1016/j.neuroimage.2010.05.045. URL: http://dx.doi.org/10.1016/j.neuroimage.2010.05.045 (visited on 05/22/2019).

[47] Boris C Bernhardt et al. "Graph-theoretical analysis reveals disrupted small-world organization of cortical thickness correlation networks in temporal lobe epilepsy." In: *Cerebral Cortex* 21.9 (Sept. 2011), pp. 2147–2157. DOI: 10.1093/cercor/bhq291. URL: http://dx.doi.org/10.1093/cercor/bhq291 (visited on 05/22/2019).

[48] Raúl Rodríguez-Cruces and Luis Concha. "White matter in temporal lobe epilepsy: clinico-pathological correlates of water diffusion abnormalities." In: *Quantitative imaging in medicine and surgery* 5.2 (Apr. 2015), pp. 264–278. DOI: 10.3978/j.issn.2223-4292.2015.02.06. URL: http://dx.doi.org/10.3978/j.issn.2223-4292.2015.02.06 (visited on 01/09/2017).

[49] Luis Concha et al. "In vivo diffusion tensor imaging and histopathology of the fimbria-fornix in temporal lobe epilepsy." In: *The Journal of Neuroscience* 30.3 (Jan. 2010), pp. 996–1002. DOI: 10.1523/{JNEUROSCI}.1619-09.2010. URL: http://dx.doi.org/10.1523/%7BJNEUROSCI%7D.1619-09.2010 (visited on 05/22/2019).

[50] Heinz-Gregor Wieser and ILAE Commission on Neurosurgery of Epilepsy. "ILAE Commission Report. Mesial temporal lobe epilepsy with hippocampal sclerosis." In: *Epilepsia* 45.6 (June 2004), pp. 695–714. DOI: 10.1111/j.0013-9580.2004.09004.x. URL: http://dx.doi.org/10.1111/j.0013-9580.2004.09004.x (visited on 05/29/2019).

8 FIGURES LEGENDS

8.1 Figure 1. Methods: multivariate analysis and unsupervised clustering

A. Multivariate analysis: Canonical correlations. Diagram of the regularized canonical correlations analysis. For each participant, the nodal network measurements associated with a brain region were concatenated to a single row vector of matrix X. Similarly, cognitive scores were combined into matrix Y. These two sets of variables were used for the rCCA, that estimates the matrices A and B, which maximize the correlation between the linear relation of each column vector of V and U. The resulting variables U_1 and V_1 are the first canonical variate and their correlation is referred as the first canonical correlation ρ_1. Columns in A describe the extent to which that canonical variate is related to a network parameter of a specific brain region, and columns in B describe the extent to which that canonical variate is present in a particular cognitive score. The canonical loadings measure the linear correlation between an original variable of X_j or Y_j and the selected canonical variate (**Figure 2.C**). **A. Inferior panel.** The regularization parameters ($\lambda 1$, $\lambda 2$ for X and Y) are applied to the covariance matrices (S_{XX}, S_{YY}). A cross-validation procedure is performed to determine optimal regularization parameters. Cross-validation with recursive search over a grid from 0 to 1 for regularization parameters tuning optimization. The search region enclosed in the blue square is seen enlarged on the right. **B. Unsupervised clustering. A)** Cognitive features as z-scores with respect to controls are shown for each patient (rows). **B)** Example of a bootstrap realization with hierarchical clustering and its selection of optimal number of clusters. **C)** Adjacency matrix of the optimal partition for each bootstrap S_{boot}. **D)** Final stability matrix S_{ij} that represents the percentage of times a subject S_i was classified similarly to subject S_j. **E)** Hierarchical agglomerative clustering is performed over the S_{ij} matrix, clustering converges on a three-subtype solution in our cohort.

8.2 Figure 2. Regularized canonical correlation solution

A. Canonical correlations for each canonical variate, each with confidence interval and significance (* and darker gray indicate statistical significance). **B.** Scatterplot of the canonical weights assigned to the cognitive scores against the network parameter of the first canonical variate for each TLE patient (U_1 versus V_1). Processing speed score (PS) is shown as size of the circles, and color represents cognitive Class. **C.** Canonical cross-loadings of the first and second canonical variates for the cognitive scores and network parameters. Loadings were obtained by correlating each of the variables directly with a canonical variate. **C-Left** panel shows the correlation between each cognitive score and the first canonical variate. The lines represent the confidence interval over the first canonical variate (x-axis). **C-Middle** panel shows the cognitive scores and network loadings on the plane of the first and second canonical variates. Network loadings are represented by color: Purple for degree, green for cluster coefficient and orange for characteristic path length. Cognitive loadings are represented in cyan: AMI-Auditory memory, VMI-visual memory, VWM-visual working memory, IMI-immediate memory, DMI-delayed memory, VCI-verbal comprehension, WMI-working memory, PS-processing speed and PR-perceptual reasoning. **C-Right** panel shows the significant network loadings of the first canonical variate, projected to the surface space and split by network measurement.

8.3 Figure 3. Differences by cognitive class

A. *Cognitive scores for TLE patients by cognitive Class.* Each patient is represented as a line indicating their normalized cognitive scores based on control, and the mean of each Class represented as a thick line. **B.** *Connectome measures.* For each metric, effect size (Cohen's D) of each Class compared to controls is projected on cortical surfaces. Significant differences corrected for multiple comparisons are outlined in cyan; white outlines represent uncorrected $p<0.025$. **C.** *Morphological Measures.* Hippocampal volumes were z-scored relative to controls. Group differences in cortical thickness and subcortical volume shown as Cohen's D effect sizes. Thickness is relative to the mean vertex value of each Class, while volume is the mean volume of each subcortical region.

9 TABLES

Table 1: Clinical data by Class

	Class 1	**Class 2**	**Class 3**
Number	9	20	5
HS % presence	**0.33***	**0.45***	**0.80***
Gender % female	0.56	0.75	0.40
Age years	28.7 (10.8)	30.9 (12.2)	26.4 (7)
Education years	14.3 (2.9)	12.3 (2.7)	**8.4 (1.3)** $*^{1,2}$
Age at onset years	19.2 (12.2)	13.8 (7.3)	8 (7.1)
Duration years	9.4 (8.7)	17.1 (14.7)	18.4 (8.3)
AED	1.3 (0.5)	1.7 (0.7)	1.6 (0.6)
Degree centrality	93.6 (3.6)	89.3 (5.6)	87.1 (4.3)
Path length $\times 10^{-4}$	31.2 (2.8)	31.3 (3.2)	**38.6 (11.6)*** ^{1,2}
Cluster coefficient	0.72 (0.01)	0.71 (0.01)	0.71 (0.01)

AED: number of antiepileptic drugs, HS, hippocampal sclerosis. Age, education, onset, duration, AEDs, degree centrality, path length, and cluster coefficient shown as mean (standard deviation). Significant difference compared to controls ($p_{adjusted} < 0.05$). Superscripts indicate significant difference with respect to the Class indicated by the number ($p_{adjusted} < 0.05$).*